

WAVE SCATTERING WEDGE IN GAP WEDGE ANTENNAE STRUCTURES.

Billel Ali Srihen¹, Jean Paul Yonnet², Malek Benslama¹

1 Department of Electronics, Laboratory of Electromagnetism and Telecommunications, University Brothers Mentouri Constantine 1, Constantine 25000, Algeria.

2 Laboratory of Electrical Engineering, Polytechnic Institute of Grenoble, University Joseph Fourier Grenoble 38000, France.

Reçu le 12 Juillet 2017 – Accepté le 12 novembre 2017

Abstract

Antenna remote sensing deals with the extraction of object information from electromagnetic wave parameters. To fully exploit the potential for quantitative information acquisition, a detailed description of microwave diffusion is required. The research on this subject was mainly devoted to the far-field analysis which assumes an incident plane wave, calculates its scattered field and evaluates the radar cross section (RCS). However, under some practical conditions, far-field analysis is not valid and near-field analysis is required. In this paper, we have given a complete analysis of the near field of a corner structure due to an incident electric field from a linear source or a plane wave in the case of Gap Photonic Antennae. The far-field model, in the case of a linear source exciting the structure, is also analyzed. The interest of this study will structure the modeling process of the fields by having a clear vision of the near field which will bring a maximum of information in the process of remote sensing to help an accurate and correct decision-making.

Keywords: Electromagnetic wave, scattering, structure, Gap Photonic Antennae.

Résumé

La télédétection d'antenne consiste à extraire des informations d'objet à partir de paramètres d'ondes électromagnétiques. Pour exploiter pleinement le potentiel d'acquisition d'informations quantitatives, une description détaillée de la diffusion par micro-ondes est nécessaire. Les recherches sur ce sujet ont été principalement consacrées à l'analyse de champ lointain qui suppose une onde plane incidente, calcule son champ diffusé et évalue la section efficace radar (RCS). Cependant, dans certaines conditions pratiques, l'analyse en champ lointain n'est pas valide et une analyse en champ proche est requise. Dans cet article, nous avons effectué une analyse complète du champ proche d'une structure d'angle due à un champ électrique incident provenant d'une source linéaire ou d'une onde plane dans le cas des antennes photoniques de Gap. Le modèle de champ lointain, dans le cas d'une source linéaire excitant la structure, est également analysé. L'intérêt de cette étude structurera le processus de modélisation des domaines en ayant une vision claire du champ proche qui apportera un maximum d'informations dans le processus de télédétection pour aider à une prise de décision précise et correcte.

Mots clés: Onde électromagnétique, diffusion, structure, antennes photoniques Gap.

ملخص

يتعامل استشعار الهوائي عن بعد مع استخلاص معلومات الكائن من معلمات الموجات الكهرومغناطيسية. للاستفادة الكاملة من إمكانية الحصول على المعلومات الكمية ، هناك حاجة إلى وصف تفصيلي لنشر الميكروويف. وقد خصص البحث في هذا الموضوع بشكل رئيسي لتحليل المجال البعيد الذي يفترض وجود موجة مستوية حادثة ، ويحسب حقله المبعثر ويقيم المقطع العرضي الراداري (RCS). ومع ذلك ، في ظل بعض الظروف العملية ، فإن التحليل البعيد المجال غير صالح والتحليل القريب من الميدان مطلوب. في هذه الورقة ، قدمنا تحليلاً كاملاً للحقل القريب لهيكل الركن بسبب حقل كهربائي حادث من مصدر خطي أو موجة مستوية في حالة فجوة الهوائيات الضوئية. كما يتم تحليل نموذج المجال البعيد ، في حالة وجود مصدر خطي مثير للهيكل. سيهتم اهتمام هذه الدراسة بعملية نمذجة الحقل من خلال الحصول على رؤية واضحة للحقل القريب والتي ستجلب أقصى قدر من المعلومات في عملية الاستشعار عن بعد للمساعدة في اتخاذ قرار دقيق وصحيح.

الكلمات المفتاحية: موجة الكهرومغناطيسية، نشر، هيكل، هوائي ضوئي Gap.

1. INTRODUCTION

The problem of electromagnetic wave scattering is very important in many applications such as remote sensing, antennas design and especially in defense applications. The research on this topic was mostly dedicated to far-field analysis which assumes an incident plane wave, computes its scattered field due to the scattered, and evaluates the Radar Cross Section (RCS) of the scatterer. When the transmitting and receiving antennas are far from the scatterer, the incident wave can be approximated by a plane wave and the scattered far field can be considered as the radiation far field due to the induced currents on the scatterer, the far-field analysis thus applies. However, in practical applications, there are many situations where the distance between the transmitting antenna and the scatterer is not large enough to treat the field reaching the scattered as a plane wave and the relative motion between the antennas and scatterer will produce Doppler frequency shift. In these conditions the far-field analysis is not valid anymore and a near-field analysis is necessary [1].

In calculating radar cross section of complex targets [2], [3] some parts of the structure can be modeled using singly curved sheets, as the wings of an aircraft for example. For electrically large bodies the Geometrical Theory of Diffraction (GTD) [4], [5] is a good high frequency technique for computing the scattering from those bodies. But, as it is well known, that method is not valid in the caustic of reflected rays which occurs for example when we illuminate with a plane wave a singly curved screen. Physical Optics (PO) has been largely used in the last years for predicting high frequency radar cross-section problems because, unlike Geometrical Optics and the GTD, the PO is valid in the transition regions and at caustics. PO can be improved using the fringe currents contribution of the edge currents of the Physical Theory of Diffraction (PTD) [6], [7].

This paper is organized as follows: Section 2 provides the scattering analysis where the RCS formulae and their approximations are derived. Field expressions for the scattering problem by a two-dimensional perfect electric conduction wedge capped with a dielectric cylinder are thus derived. In section 3, some numerical results for various configurations of the wedge structure are presented. Finally, Section 4 concludes our investigation.

Compared to conventional methods that allow analyzing the near field, i.e. Physical Optics and Physical Theory of Diffraction, an important scale can appear, it is due to the caustics, their computation made from the functions of Airy is extremely tedious, and it can distort the measurement of amplitudes in near field. This is the main motivation that prompted us to use the Radar Cross section [2].

We note that references (6) and (7) give approximate results, and the analysis of these results in a practical context is extremely difficult. It should be noted that practically it is radar which is used to travel the signal and to recover it. The choices made by references (6) and (7)

are difficult to adapt to functional radar used for remote sensing.

2- SCATTERING ANALYSIS

The RCS of a target characterizes its scattering property, which is defined as the area intercepting the amount of power that, when scattered isotropically, produces in a receiver a density that is equal to the density scattered by the actual target. When the transmitter and receiver are in the same location, the RCS is referred to as monostatic (or backscattered), and it is referred to as bistatic when the two are located at different positions.

For three-dimensional target, the RCS is given in terms of incident power density, magnetic field, and electric field [8]. The RCS in terms of electric field is given by:

$$\sigma_{3-D} = \lim_{\rho \rightarrow \infty} \left[4\pi\rho^2 \frac{|E^s|^2}{|E^i|^2} \right] \quad (1)$$

Where ρ is the distance from target to the observation point, E^s and E^i are scattered and incident electric field respectively. Equation (1) is valid when the target is illuminated by a plane wave which in practice can be only approximated when the target is placed in the far field of the source, i.e. at least $\rho = 2D^2/\lambda$, where D is the largest dimension of the target.

A perfectly conducting rectangular thin flat plate in the $x - y$ plane as shown in Fig.1 is considered for our calculations.

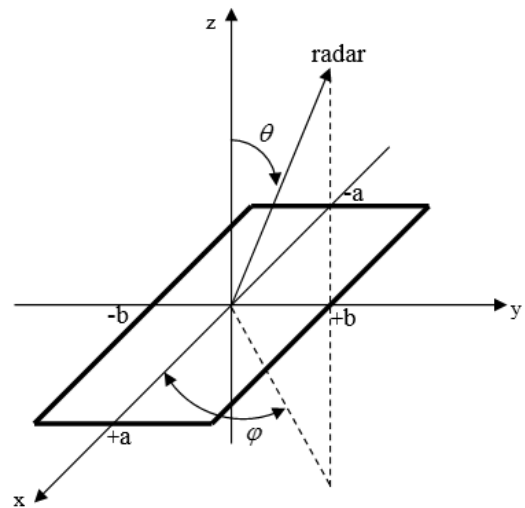


Fig. 1 coordinates for rectangular flat plate.

For a linearly polarized incident wave in the $x - y$ plane, the horizontal and vertical backscattered radar cross sections are respectively given by:

$$\sigma_V = \frac{b^2}{\pi} \left| \sigma_{1V} - \sigma_{2V} \left[\frac{1}{\cos \theta} + \frac{\sigma_{2V}}{4} (\sigma_{3V} + \sigma_{4V}) \sigma_{5V}^{-1} \right] \right|^2 \quad (2)$$

$$\sigma_H = \frac{b^2}{\pi} \left| \sigma_{1H} - \sigma_{2H} \left[\frac{1}{\cos \theta} - \frac{\sigma_{2H}}{4} (\sigma_{3H} + \sigma_{4H}) \sigma_{5H}^{-1} \right] \right|^2 \quad (3)$$

Where σ_{iV} and σ_{iH} (with $i=1,..4$) are detailed in appendices.

Wherein $k_a = k_0 \cdot a$, k_0 is the free space wave number. Eqs. (2) and (3) are accurately valid for aspect angles $0^\circ \leq \theta \leq 80^\circ$. For aspect angles near 90° , Ross [9] obtained by extensive fitting of measured data an empirical expression for the radar cross section. The latter is given by:

$$\sigma_H \rightarrow 0$$

$$\sigma_V = \frac{ab}{\lambda} \left\{ \left[1 + \frac{\pi}{2(2a/\lambda)^2} \right] + \left[1 - \frac{\pi}{2(2a/\lambda)^2} \right] \cos \left(2k_a - \frac{3\pi}{5} \right) \right\} \quad (4)$$

The backscattered RCS for a perfectly conducting thin rectangular plate for incident waves at any θ , φ can be approximated by:

$$\sigma = \frac{4\pi a^2 b^2}{\lambda^2} \left(\frac{\sin(ak_0 \sin \theta \cos \varphi) \sin(bk_0 \sin \theta \cos \varphi)}{ak_0 \sin \theta \cos \varphi \quad bk_0 \sin \theta \cos \varphi} \right)^2 (\cos \theta)^2 \quad (5)$$

Eq.(5) is independent of the polarization, and it is only valid for aspect angles $\theta \leq 20^\circ$. Fig.2 shows the backscattered RCS of a rectangular flat plate, for both vertical and horizontal polarisations.

Fig.2 presents the radar cross section of a rectangular flat plate for the vertical and horizontal polarizations, compared with the classical formulae. The parameters of structure are $a = b = 10.16$ cm and $f = 300$ MHz.

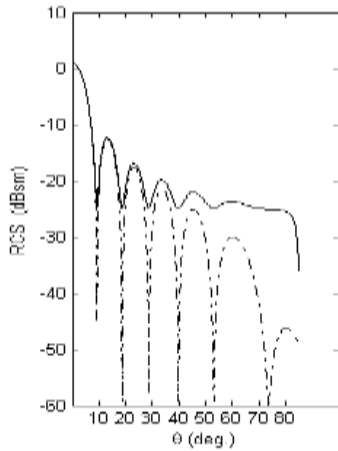


Fig. 2a Backscattered RCS for a rectangular flat plate Vertical polarization

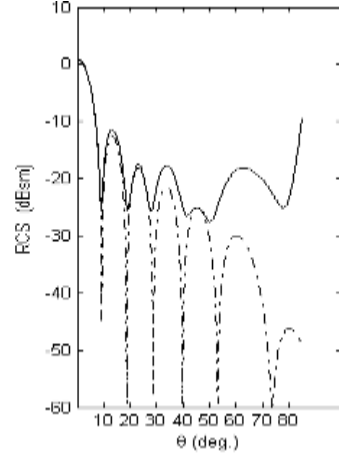


Fig. 2b Backscattered RCS for a rectangular flat plate horizontal polarization.

The goal of our analysis is to find the field expressions for the problem of scattering by a two-dimensional (2-D) perfect electric conduction (PEC) wedge capped with a dielectric cylinder as shown in Fig.3.

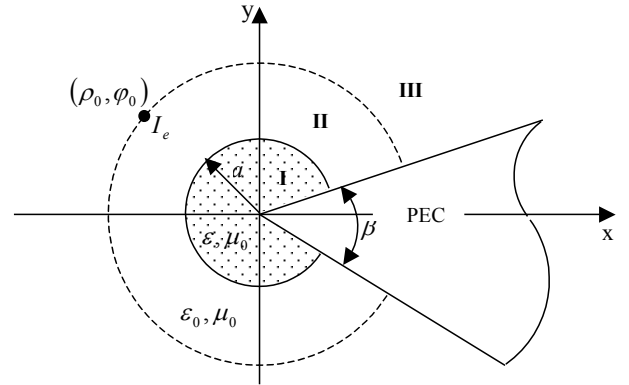


Fig. 3 Capped wedge structure.

Using the cylindrical coordinates system, the excitation due to an electric line current of amplitude I_e located at (ρ_0, φ_0) result in transverse magnetic (TM) incident field with the electric field expression given by

$$E_z^i = -I_e \frac{\omega \mu_0}{4} H_0^{(2)}(k_0 |\rho - \rho_0|) \quad (7)$$

Where $H_0^{(2)}$ is the Hankel function of the second kind of zero order.

The problem is divided into three regions I, II, and III. The field expressions may be assumed to take the following forms:

$$\begin{aligned}
 E_z^I &= \sum_{n=0}^{\infty} a_n J_\nu(k_1 \rho) \sin \nu(\varphi - \alpha) \sin \nu(\varphi_0 - \alpha) \\
 E_z^{II} &= \sum_{n=0}^{\infty} (b_n J_\nu(k_0 \rho) + c_n H_\nu^{(2)}(k_0 \rho)) \sin \nu(\varphi - \alpha) \sin \nu(\varphi_0 - \alpha) \\
 E_z^{III} &= \sum_{n=0}^{\infty} d_n H_\nu^{(2)}(k_0 \rho) \sin \nu(\varphi - \alpha) \sin \nu(\varphi_0 - \alpha)
 \end{aligned} \tag{8}$$

Where k_1 is the wave number inside the dielectric medium.

$$\nu = \frac{n\pi}{2\pi - \alpha - \beta} \tag{9}$$

While $J_\nu(x)$ and $H_\nu^{(2)}$ are, respectively, the Bessel and Hankel functions of order ν and argument x . From Maxwell equations, the magnetic field component H_φ is related to the electric field component E_z for a TM wave by:

$$H_\varphi = \frac{1}{j\omega\mu} \frac{\partial E_z}{\partial \rho} \tag{10}$$

Thus, the magnetic field component H_φ in the various regions may be written as:

$$\begin{aligned}
 H_\varphi^I &= \frac{k_1}{j\omega\mu_0} \sum_{n=0}^{\infty} a_n J_\nu'(k_1 \rho) \sin \nu(\varphi - \alpha) \sin \nu(\varphi_0 - \alpha) \\
 H_\varphi^{II} &= \frac{k_0}{j\omega\mu_0} \sum_{n=0}^{\infty} (b_n J_\nu'(k_0 \rho) + c_n H_\nu^{(2)'}(k_0 \rho)) \sin \nu(\varphi - \alpha) \sin \nu(\varphi_0 - \alpha) \\
 H_\varphi^{III} &= \frac{k_0}{j\omega\mu_0} \sum_{n=0}^{\infty} d_n H_\nu^{(2)'}(k_0 \rho) \sin \nu(\varphi - \alpha) \sin \nu(\varphi_0 - \alpha)
 \end{aligned} \tag{11}$$

The boundary conditions require that the tangential electric field components vanish at the PEC surface. Also the tangential field components should be continuous across the air-dielectric surface and the virtual boundary between regions I and II, except for the discontinuity of the magnetic field at the source point. Thus,

$$E_z = 0 \text{ at } \varphi = \alpha, 2\pi - \beta \tag{12}$$

$$\begin{cases} E_z^I = E_z^{II} \\ H_\varphi^I = H_\varphi^{II} \end{cases} \text{ at } \rho = a \tag{13}$$

$$\begin{cases} E_z^{II} = E_z^{III} \\ H_\varphi^{II} = H_\varphi^{III} \end{cases} \text{ at } \rho = \rho_0 \tag{14}$$

The current density J_e may be given in Fourier series expansion as

$$J_e = \frac{I_e}{\rho_0} \delta(\varphi - \varphi_0) = \frac{2}{2\pi - \alpha - \beta} \frac{I_e}{\rho_0} \sum_{n=0}^{\infty} \sin \nu(\varphi - \alpha) \sin \nu(\varphi_0 - \alpha) \tag{15}$$

The boundary condition on the PEC surface is automatically satisfied by the φ dependence of the electric field Eq.(8). From the boundary conditions in Eq.(13)

$$\sum_{n=0}^{\infty} a_n J_\nu(k_{1a}) \sin \nu(\varphi - \alpha) \sin \nu(\varphi_0 - \alpha) = \sum_{n=0}^{\infty} (b_n J_\nu(k_a) + c_n H_\nu^{(2)}(k_a)) \sin \nu(\varphi - \alpha) \sin \nu(\varphi_0 - \alpha) \tag{17}$$

$$\frac{k_1}{j\omega\mu_0} \sum_{n=0}^{\infty} a_n J_\nu'(k_{1a}) \sin \nu(\varphi - \alpha) \sin \nu(\varphi_0 - \alpha) = \frac{k_0}{j\omega\mu_0} \sum_{n=0}^{\infty} (b_n J_\nu'(k_a) + c_n H_\nu^{(2)'}(k_a)) \sin \nu(\varphi - \alpha) \sin \nu(\varphi_0 - \alpha) \tag{18}$$

From the boundary conditions in Eq.(15), we have:

$$\sum_{n=0}^{\infty} (b_n J_\nu(k_0 \rho_0) + c_n H_\nu^{(2)}(k_0 \rho_0)) \sin \nu(\varphi - \alpha) \sin \nu(\varphi_0 - \alpha) = \sum_{n=0}^{\infty} d_n H_\nu^{(2)}(k_0 \rho_0) \sin \nu(\varphi - \alpha) \sin \nu(\varphi_0 - \alpha) \tag{19}$$

$$\begin{aligned}
 &\frac{k}{j\omega\mu_0} \sum_{n=0}^{\infty} (b_n J_\nu'(k_0 \rho_0) + c_n H_\nu^{(2)'}(k_0 \rho_0)) \sin \nu(\varphi - \alpha) \sin \nu(\varphi_0 - \alpha) = \\
 &\frac{k}{j\omega\mu_0} \sum_{n=0}^{\infty} d_n H_\nu^{(2)'}(k_0 \rho_0) \sin \nu(\varphi - \alpha) \sin \nu(\varphi_0 - \alpha) - \frac{2}{2\pi - \alpha - \beta} \frac{I_e}{\rho_0} \sum_{n=0}^{\infty} \sin \nu(\varphi - \alpha) \sin \nu(\varphi_0 - \alpha)
 \end{aligned} \tag{20}$$

Since Eqs.(17) and (20) hold for all φ , the series of the left and right hand sides should be equal term by term. That is to say,

$$a_n J_\nu(k_{1a}) = b_n J_\nu(k_a) + c_n H_\nu^{(2)}(k_a) \tag{21}$$

$$k_1 a_n J_\nu'(k_{1a}) = k (b_n J_\nu'(k_a) + c_n H_\nu^{(2)'}(k_a)) \tag{22}$$

$$b_n J_\nu(k_0 \rho_0) + c_n H_\nu^{(2)}(k_0 \rho_0) = d_n H_\nu^{(2)}(k_0 \rho_0) \tag{23}$$

$$b_n J_\nu'(k_0 \rho_0) + c_n H_\nu^{(2)'}(k_0 \rho_0) = d_n H_\nu^{(2)'}(k_0 \rho_0) - \frac{2j\eta_0}{2\pi - \alpha - \beta} \frac{I_e}{\rho_0} \tag{24}$$

Where η_0 is the characteristic impedance of free space.

From Eqs.(21) and (23), we have

$$a_n = \frac{1}{J_\nu(k_{1a})} [b_n J_\nu(k_a) + c_n H_\nu^{(2)}(k_a)] \quad (25)$$

$$d_n = c_n + b_n \frac{J_\nu(k_0 \rho_0)}{H_\nu^{(2)}(k_0 \rho_0)} \quad (26)$$

After some mathematical calculations, we get:

$$b_n = -\frac{\pi \omega \mu_0 I_e}{2\pi - \alpha - \beta} H_\nu^{(2)}(k_0 \rho_0) \quad (27)$$

Substituting b_n in Eqs.(21) and (22) and solving for c_n yields:

$$c_n = \frac{\pi \omega \mu_0 I_e}{2\pi - \alpha - \beta} \left[H_\nu^{(2)}(k_0 \rho_0) \frac{k_0 J'_\nu(k_a) J_\nu(k_{1a}) - k_1 J_\nu(k_a) J'_\nu(k_{1a})}{k_0 H_\nu^{(2)}(k_a) J_\nu(k_{1a}) - k_1 H_\nu^{(2)}(k_a) J'_\nu(k_{1a})} \right] \quad (28)$$

From Eqs.(26) through (28), d_n may be given by:

$$d_n = \frac{\pi \omega \mu_0 I_e}{2\pi - \alpha - \beta} \left[H_\nu^{(2)}(k_0 \rho_0) \frac{k_0 J'_\nu(k_a) J_\nu(k_{1a}) - k_1 J_\nu(k_a) J'_\nu(k_{1a})}{k_0 H_\nu^{(2)}(k_a) J_\nu(k_{1a}) - k_1 H_\nu^{(2)}(k_a) J'_\nu(k_{1a})} - J_\nu(k_0 \rho_0) \right] \quad (29)$$

with these closed form expressions for the expansion coefficients a_n , b_n , c_n and d_n , the field components E_z and H_φ can be determined from Eq.(9) and Eq.(12), respectively. Alternatively, the magnetic field component H_ρ can be computed from

$$H_\rho = -\frac{1}{j\omega\mu} \frac{1}{\rho} \frac{\partial E_z}{\partial \varphi} \quad (30)$$

Thus, the H_ρ expressions for the three regions defined in Fig.2 become:

$$\begin{aligned} H_\rho^I &= -\frac{1}{j\omega\mu\rho} \sum_{n=0}^{\infty} a_n \nu J_\nu(k_1 \rho) \cos \nu(\varphi - \alpha) \sin \nu(\varphi_0 - \alpha) \\ H_\rho^{II} &= -\frac{1}{j\omega\mu\rho} \sum_{n=0}^{\infty} \nu (b_n J_\nu(k_0 \rho) + c_n H_\nu^{(2)}(k_0 \rho)) \cos \nu(\varphi - \alpha) \sin \nu(\varphi_0 - \alpha) \\ H_\rho^{III} &= -\frac{1}{j\omega\mu\rho} \sum_{n=0}^{\infty} d_n \nu H_\nu^{(2)}(k_0 \rho) \cos \nu(\varphi - \alpha) \sin \nu(\varphi_0 - \alpha) \end{aligned} \quad (31)$$

In region III, the far scattered field may be found as the difference between the total and incident field. Thus, using Eqs.(8) and (9) and considering the far field condition ($\rho \rightarrow \infty$) we get:

$$E_z^{III} = E_z^i + E_z^s = \sqrt{\frac{2j}{\pi k_0 \rho}} e^{-jk_0 \rho} \sum_{n=0}^{\infty} d_n j^\nu \sin \nu(\varphi - \alpha) \sin \nu(\varphi_0 - \alpha) \quad (32)$$

For a plane wave excitation ($\rho_0 \rightarrow \infty$), the expressions in Eqs. (27) and (28) simplify to:

$$b_n = -\frac{\pi \omega \mu_0 I_e}{2\pi - \alpha - \beta} j^\nu \sqrt{\frac{2j}{\pi k_0 \rho_0}} e^{-jk_0 \rho_0} \quad (33)$$

$$c_n = \frac{\pi \omega \mu_0 I_e}{2\pi - \alpha - \beta} j^\nu \sqrt{\frac{2j}{\pi k_0 \rho_0}} e^{-jk_0 \rho_0} \frac{k_0 J'_\nu(k_a) J_\nu(k_{1a}) - k_1 J_\nu(k_a) J'_\nu(k_{1a})}{k_0 H_\nu^{(2)}(k_a) J_\nu(k_{1a}) - k_1 H_\nu^{(2)}(k_a) J'_\nu(k_{1a})} \quad (34)$$

Where the complex of the incident plane wave, E_0 , can be given by:

$$E_0 = -I_e \frac{\omega \mu_0}{4} \sqrt{\frac{2j}{\pi k_0 \rho_0}} e^{-jk_0 \rho_0} \quad (35)$$

In this case, the field components can be evaluated in regions I and II only.

3- Numerical results and discussion :

The previous formulas have been programmed on Matlab, they give us the following results reported in the figures below.

Fig.4 presents the far field of a capped wedge in the presence of an electric line source field. We clearly show how the cap parameters affect the maximum radiation of the line source in the presence of wedge.

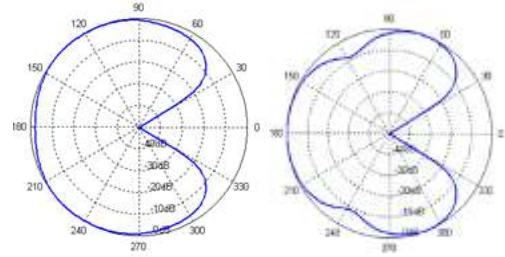


Fig. 4: Total far field pattern of a line source near a conducting wedge.

(a) conducting-capped edge. (b) dielectric-capped edge.

The distribution of the components of the fields on the near field of two cases (conducting capped edge, dielectric capped edge) is computed and shown in Figs.5&6.

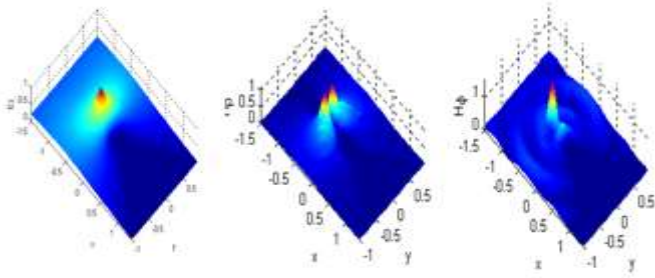


Fig. 5 Near field patterns of a line source near a conducting wedge with conducting-capped edge (a) E_z (b) H_ρ (c) H_ϕ .

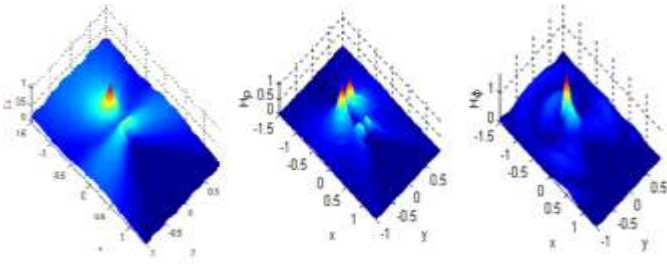


Fig. 6 Near field patterns of a line source near a conducting wedge with dielectric-capped edge (a) E_z (b) H_ρ (c) H_ϕ .

The near field distribution for an incident wave field of the two types of wedges is also computed and shown in Figs.7&8. These near field distributions clearly demonstrated the effect of cap parameters in altering the sharp edge singular behaviour. We have used the following wedge structure parameters:

$$a = 0.15 \text{ m}, \rho_0 = 0.5 \text{ m}, \alpha = \beta = 30^\circ, \epsilon_r = 3, I_e = 1 \text{ mA}$$

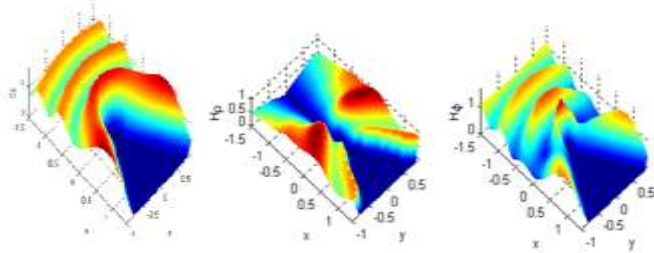


Fig. 7 Near field patterns of plane wave incident on a conducting wedge with conducting-capped edge (a) E_z (b) H_ρ (c) H_ϕ .

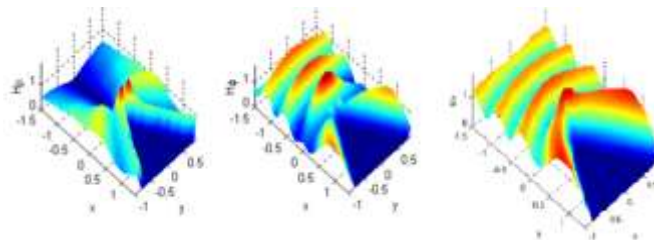


Fig. 8 Near field patterns of plane wave incident on a conducting wedge with dielectric-capped (a) E_z (b) H_ρ (c) H_ϕ .

CONCLUSION

In this paper, we have presented a full analysis of electromagnetic scattering. We have dealt with a case of backscattered radar cross section for a rectangular flat plate. An analysis of the far and near field patterns for a wedge structure shows the effect of cap parameters on the maximum radiation of the line source. We have also examined the effect of the cap parameters on the sharp edge behavior for an incident plane wave.

APPENDICES:

$$\sigma_{1V} = \cos(k_a \sin \theta) - j \frac{\sin(k_a \sin \theta)}{\sin \theta}$$

$$\sigma_{2V} = \frac{e^{j(ka - \pi/4)}}{\sqrt{2\pi}(k_a)^{3/2}}$$

$$\sigma_{3V} = \frac{(1 + \sin \theta)e^{-jk_a \sin \theta}}{(1 - \sin \theta)^2}$$

$$\sigma_{4V} = \frac{(1 - \sin \theta)e^{jk_a \sin \theta}}{(1 + \sin \theta)^2}$$

$$\sigma_{5V} = 1 - \frac{e^{j(2k_a - \pi/2)}}{8\pi(k_a)^3}$$

$$\sigma_{1H} = (\sigma_{1V})^*$$

$$\sigma_{2H} = \frac{4e^{j(k_a + \pi/4)}}{\sqrt{2\pi}(k_a)^{1/2}}$$

$$\sigma_{3H} = \frac{e^{-jk_a \sin \theta}}{1 - \sin \theta}$$

$$\sigma_{4H} = \frac{e^{jk_a \sin \theta}}{1 + \sin \theta}$$

$$\sigma_{5V} = 1 - \frac{e^{j(2k_a + \pi/2)}}{2\pi(k_a)}$$

REFERENCES:

1. J.M Le Caillec, S.Redadaa, C.Sintes, B. Solaiman and M.Benslama : Focusing Problems of a buried point scatterer using a low frequency SAR. IEEE transactions on Aerospace and Electronic Systems, Vol 47, N°1, January 2011, pp438-453.
2. Zaakouf; S. Readaa, M.Benslama: Closed form of topographic elevation in the context of interferometric synthetic aperture. International Journal of Numerical Modeling, Electronic Networks, Devices and Field, Volume 30, Issue 2, March/April 2017.
3. Colton D. and Kress R. *Integral equation methods in scattering theory*; Wiley: Intersciences New York, 1983.

4. Kouyoumjian R. G and P. H Pathak P. H. A uniform geometrical theory of diffraction for an edge in a perfectly conducting surface. *Proceedings IEEE* 1974; **62** (11), 1448- 1461.
5. Rao S. M, .Wilton D. R and Glisson A. W. Electromagnetic scattering by surfaces of arbitrary shape. *IEEE Transactions on Antenna and Propagation* 1982; **30**(3), 409-418.
6. Knott E.F, Shaeffer J.F and Tuley M.T. *Radar cross section: Its prediction, measurement and reduction*, Dedham, MA: Artech House, 1985.
7. Blume S and Krebs V, Numerical evaluation of dyadic diffraction coefficients and bistatic radar cross sections for a perfectly conducting semi-infinite elliptic cone. *IEEE Transactions on Antenna and Propagation* 1998; **46**(3), 414-424.
8. Balanis C. A. *Antenna theory: Analysis and design*, John Wiley & Sons, 2nd edition, New York, 1997.
9. Ross R.A. Radar cross section of rectangular flat plate as function of aspect angle. *IEEE Transactions on Antenna and Propagation* 1966; **14**, 329-335.